Letter of Intent

Polarization Observables in the Photoproduction of Hyperons using a Polarized Photon Beam and a Polarized Target

L. Todor[1], R. Schumacher[1], J. Kellie[2], W.J. Briscoe[3], I. Strakovsky[3],
H. Crannell[4], F.J. Klein[4], D.I. Sober[4], J.C. Sanabria[5]

[1] Carnegie Mellon University, Pittsburgh, PA 15213
[2] University of Glasgow, G12 8QQ, Glasgow, United Kingdom
[3] The George Washington University, Washington, DC 20064
[4] The Catholic University of America, Washington, DC 20052
[5] Universidad de los Andes, A.A. 4976, Santafé de Bogotá, Colombia

Abstract

We propose to measure single and double polarization observables in associated strangeness production using polarized targets. The final goal of this experiment, in concert with the **C**LAS **A**pproved **A**nalysis of $\vec{\gamma} p \to K^+ \vec{\Lambda}$, is to perform a complete set of measurements for ground-state hyperon photoproduction in the reactions $\gamma p \to K^+\Lambda$, $\gamma p \to K^+\Sigma^0$, and $\gamma p \to K^0\Sigma^+$.

Due to the weak decay of Λ and Σ^+, the **recoil** polarization can be determined in coincidence with polarization states of the incoming particles: **beam photon** and **target proton**. This allows – for each reaction – to determine seven independent observables which fully describe these reaction channels. Additionally, we will measure a broad range of double polarization observables which are connected via algebraic functions but will allow for extensive checks of systematics.

Calculations based on various isobar models show that polarization observables involving beam and target polarization are most sensitive to s-channel contributions, e.g. contributions of N^* or Δ^* states.

1 Introduction

The detailed study and understanding of the excitation spectrum of the nucleon is required to describe the underlying interactions. The nonperturbative nature of QCD at low energies has represented a major challenge to hadronic physics, and made it unavoidable to use phenomenological quark models. In these models, the internal structure of the nucleon is represented by three constituent valence quarks interacting with each other through a potential [1, 2]. The number of nucleon resonances predicted by quark models based on the SU(6)$\times$O(3) symmetry is larger than the number of the experimentally observed ones. Why there are many resonances *missing* in the experimental spectrum is a current problem in this field.

Recently, a detailed study by Capstick and Roberts [3] on the decay of nucleon resonances into a strange baryon and a strange meson, suggests that some of the so called "missing" resonances may couple strongly to $\mathrm{K}^+\Lambda$ and $K\Sigma$. Since $\mathrm{K}^+\Lambda$ photoproduction can only involve isospin 1/2 resonances, one expects that only a few of those states contribute to the s-channel for the reaction $\gamma p \to K^+\Lambda$. Therefore, the analysis required to identify the contributing N^* resonances should be simpler than for other channels. On the other hand, the additional analysis of the two isospin states of $\Sigma(1192)$ allows for a more complete understanding of associated strangeness production. Capstick and Roberts predict that the signature of some missing resonances can be observed in these processes, and particularly the $D_{13}(1960)$ resonance should clearly be visible in $\gamma p \to K^+\Lambda$.

The most recent data for the total cross section of the reaction $\gamma p \to K^+\Lambda$, coming from SAPHIR [4], shows an enhancement in the $\mathrm{K}^+\Lambda$ channel at a center-of-mass energy W of about 1.9 GeV. A calculation by Mart and Bennhold [5] finds a resonance with a mass of 1895 MeV, and interpret this structure in the SAPHIR cross section as the result of the contribution of the $D_{13}(1960)$ resonance. Mart and Bennhold also point out that the presence of particular resonances in the s-channel should have large effects on polarization observables. One should also bear in mind that besides the $D_{13}(1960)$ resonance, Capstick and Roberts predict sizeable contributions from other *missing* resonances at slightly higher W.

The use of polarized photon beams, together with longitudinally and/or transversely polarized targets, and the measurement of the polarization of the recoiling hyperon will provide a complete set of measurements for the reactions $\gamma p \to K^+\Lambda$, $\gamma p \to K^0\Sigma^+$, and $\gamma p \to K^+\Sigma^0$. In combination with data (i) taken during the CLAS-g8 run period, using a beam of linearly polarized photons, and (ii) taken during the CLAS-g1 run period, using a beam of circularly polarized photons, more than the required seven independent observables can be determined for all three reactions. Making use of the algebraic correlations between various polarization observables will allow for consistency tests for all three data sets. The proposed measurements will faciliate a model-independent partial wave analysis (PWA) of these reactions to identify intermediate N^* (and Δ^*, Λ^*) resonances.

2 Previous Measurements

The experimental study of the photoproduction of kaons started in the late 1950s, and was pursued until the early 1970s [6, 7]. The data extended from threshold up to 1.4 GeV.[1] Several sets of differential cross section data, a few total cross sections as well as hyperon polarization and polarized target measurements exist.

Twenty years later, new data for this reaction was obtained at the electron stretcher ring ELSA in Bonn using the SAPHIR detector [10]. Initially, SAPHIR collected data for the reactions $\gamma p \to K^+\Lambda$ and $\gamma p \to K^0\Sigma^+$ up to a photon energy of 1.47 GeV [11]. Recently, SAPHIR has acquired a new set of data that goes from threshold up to 2 GeV photon energy [4]. This new data set is of higher quality than the previous one, allowing structures in the total cross section to be observed as a function of energy.

In Fig. 5, the SAPHIR data for $\gamma p \to K^+\Lambda$ is displayed as a function of the center-of-mass energy $W = \sqrt{s}$. The plot shows the cross section rising quickly from threshold up to its maximum at $W \approx 1.7$ GeV, and then decreasing. This general shape has a structure at about 1.9 GeV with a width of about 0.2 GeV superimposed on it. The presence of this structure in the SAPHIR data may be interpretated as experimental evidence of the excitation for an undiscovered baryon resonance.

A new data set obtained at Jefferson Laboratory using unpolarized and circularly polarized photon beams and the CLAS detector is currently being analyzed. The final results from this experiment (E-89-004 [12] as part of CLAS-g1) are expected to reveal any structure in the total cross section with improved accuracy. Preliminary results were presented at several workshops and conferences. Figure 1 shows the total cross section as a function of the c.m. energy W in comparison with several model predictions. The evolution of the $K^+\Lambda$ cross section confirms the general behavior of the SAPHIR results. On the other hand, we can see from the plot that none of the model predictions describe the evolution of the measured cross section above $W \simeq 1.95$ GeV.

[1] Exceptions were cross section data at much higher photon energies: 4.0 GeV [8] and 20 GeV [9].

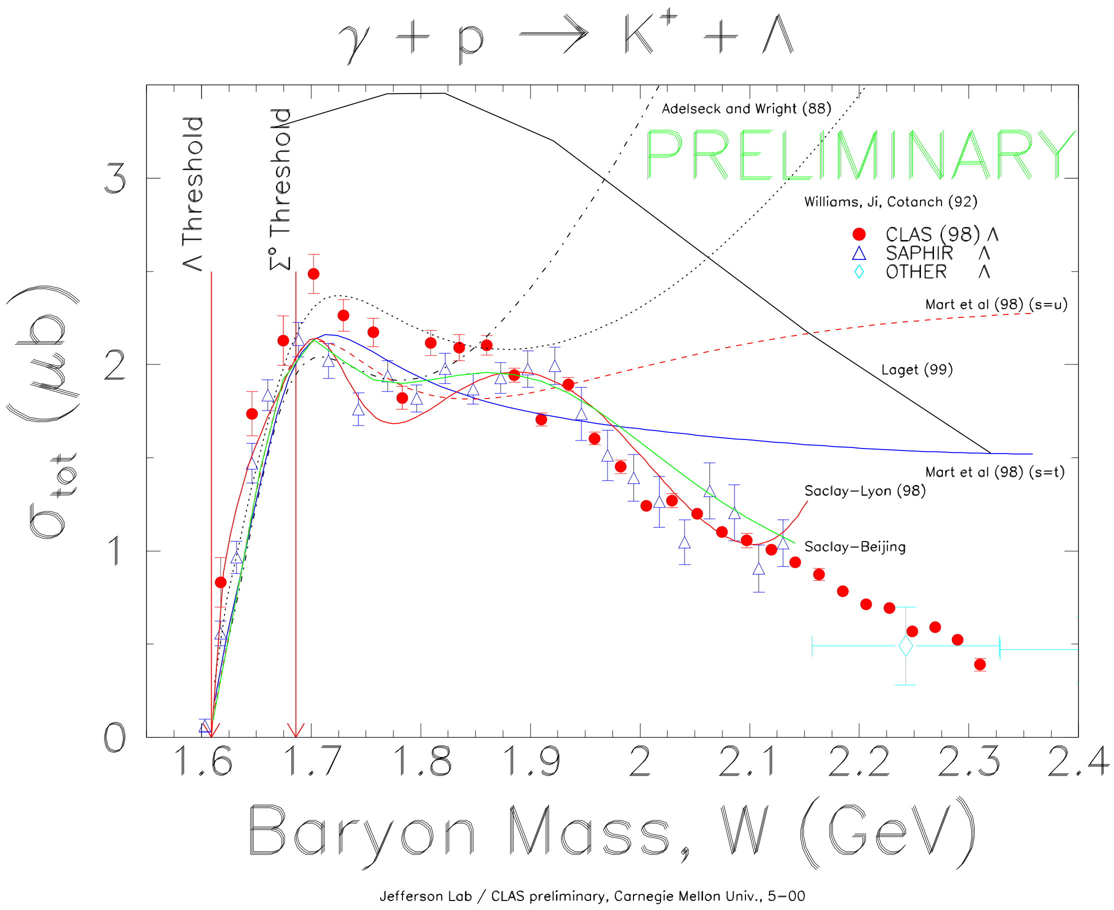

Figure 1: Preliminary cross section for $\gamma p \rightarrow K^+\Lambda$ from CLAS in comparison with various model predictions. The data was taken in 1998 (`g1a` running period).

In the case of polarized beam and target observables, the existing data is sparse and fragmentary, and for several observables there are no data at all. In fact, the current database for the reaction $\gamma p \rightarrow K^+\Lambda$ is not sufficient for a model independent analysis (PWA) which requires significantly more measurements. The GW00 energy dependent solution was recently performed for $E_\gamma = 920 - 1600$ MeV [13], but it was found that the solution is not stable over a broad energy range because of the lack of data. The distribution of available data is given in Fig. 2.

The following data points are available:

Observable:	E_γ=0.92–1.6 GeV,	E_γ=1.6–2.4 GeV
differential cross section:	323 data points,	30 data points
total cross section:	32	8
recoil polarization:	53	6
target polarization:	3	0

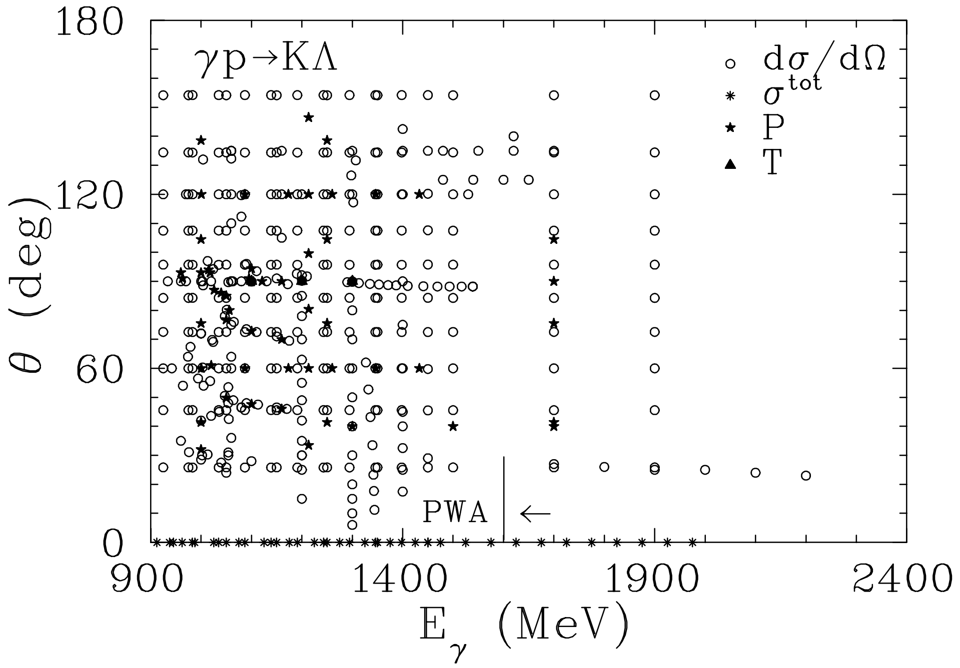

Figure 2: The current database of observables for the reaction $\gamma p \to K^+\Lambda$.

3 Theoretical Formalism

The theoretical description of the associated production of strange particles has been pursued for more than four decades, but the underlying reaction mechanism is still not well understood. This might be attributed to the complex role played by the *strange* quark. This new degree-of-freedom – in addition to those of *up* and *down* quark – can result in the excitation of several nucleon and hyperon resonances that are not present in pion photoproduction.

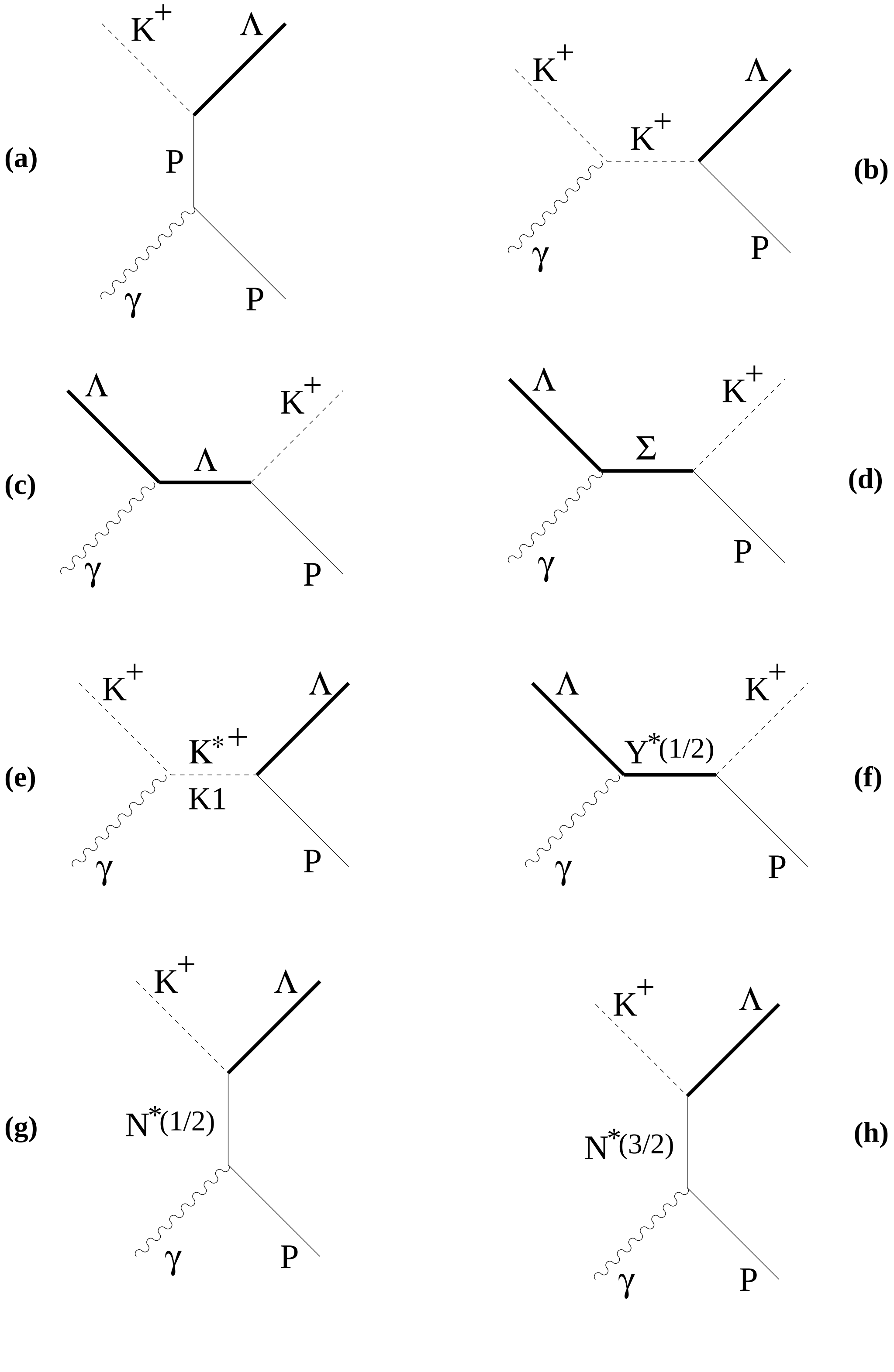

Figure 3: Feynman diagrams for the process $\gamma p \to K^+\Lambda$.

The phenomenological description of kaon photoproduction has been based on dynamical models using hadronic degrees of freedom. Most of the analyses have been done at the tree level, providing a simple tool to parametrize the reaction by some unkown coupling parameters (coupling constants) that are adjusted in order to reproduce the experimental data.

In a tree-level isobar model, the Feynman diagrams contributing to this process are shown in Fig. 3. Diagrams (a) through (d) constitute the Born terms, diagrams (e) through (f) constitute non-resonant background, and diagrams (g) and (h) constitute the spin 1/2 and spin 3/2 resonant terms in the s-channel.

The coordinate systems and kinematical variables used in the description of these reactions in the center-of-mass reference frame are defined in Figure 4.

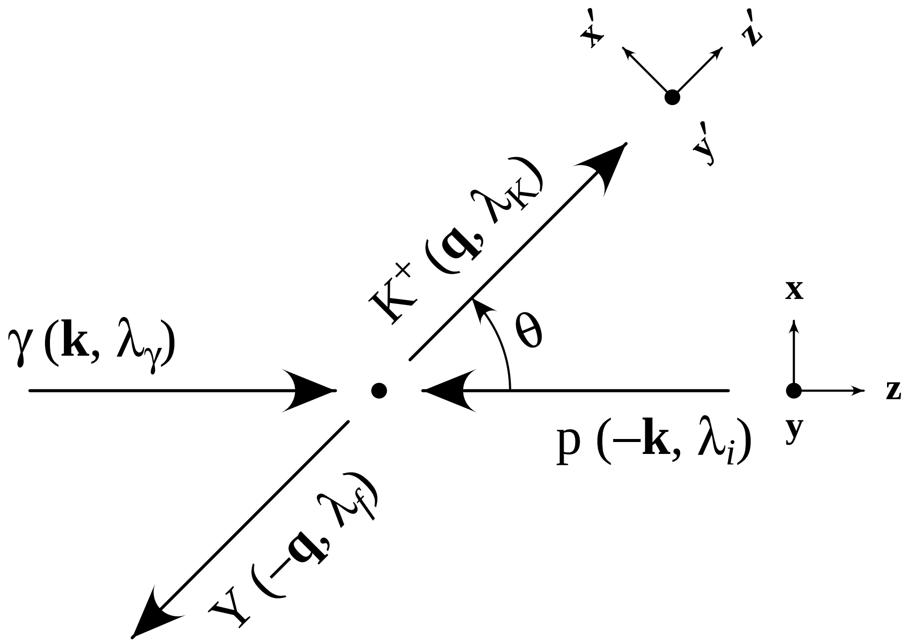

Figure 4: Coordinate systems and kinematical variables for Kaon photoproduction.

The differential cross section has the form

$$\frac{d\sigma}{d\Omega_{cm}} = \frac{(E_p + M_p)(E_Y + M_Y)}{128\pi^2 s} \frac{|\,\mathbf{q}\,|}{|\,\mathbf{k}\,|} Tr(\mathcal{F}\mathcal{F}^\dagger) \ , \tag{1}$$

where $\mathbf{k}$ is the incoming photon momentum, $\mathbf{q}$ is the outgoing Kaon momentum in the center-of-mass frame, and $\mathcal{F}$ is defined as

$$\mathcal{F} = f_1 \boldsymbol{\sigma}\cdot\boldsymbol{\epsilon} + i f_2 \frac{(\boldsymbol{\sigma}\cdot\boldsymbol{q})(\boldsymbol{\sigma}\cdot\ \boldsymbol{k}\times\boldsymbol{\epsilon})}{|\,\mathbf{q}\,||\,\mathbf{k}\,|} + f_3 \frac{(\boldsymbol{\sigma}\cdot\boldsymbol{k})(\boldsymbol{q}\cdot\boldsymbol{\epsilon})}{|\,\mathbf{q}\,||\,\mathbf{k}\,|} + f_4 \frac{(\boldsymbol{\sigma}\cdot\boldsymbol{q})(\boldsymbol{q}\cdot\boldsymbol{\epsilon})}{\mathbf{q}^2} \ , \tag{2}$$

where the f_i are the Chew, Goldberger, Low, and Nambu (CGLN) amplitudes [14], and ϵ is the polarization vector of the photon.

The set of experiments that completely describes the reaction $\gamma p \to K^+\Lambda$ consists of measurements using unpolarized beam, circularly polarized beam, linearly polarized beam, unpolarized target, and polarized target. If one also measures the polarization vector of the recoiling hyperon, a total of 16 observables can be obtained.[2] These observables produce redundant information that is reflected by nonlinear relations among them. For example, the expressions

$$C_x^2 + C_z^2 + O_x^2 + O_z^2 = 1 + T_y^2 - P_y^2 - \Sigma_x^2 \tag{3}$$

$$C_z O_x - C_x O_z = T_y - P_y \Sigma_x \ , \tag{4}$$

relate the observables obtained in a linearly-polarized-beam experiment (Σ_x, O_x, O_z) with the observables C_x and C_z that are measured directly in a circularly-polarized-beam experiment. The reaction is described by four complex CGLN amplitudes but there is an overall arbitrary phase factor that reduces the number of independent quantities to 7. A complete set of independent observables requires the measurement of polarization observables involving a polarized target.

4 Theoretical Predictions

In the range of photon energies available at Jefferson Lab, the electromagnetic production of kaons is expected to result in part from the excitation of non-strange baryons in the s-channel, which subsequently decay into a strange baryon and a strange meson [3]. The constituent quark model of Capstick and Roberts [2] predicts many new excited baryon states in this energy range that have not been seen in πN elastic and inelastic scattering; however, only a few of them have a significant $K^+\Lambda$ decay width. In Table 1 the photoproduction amplitudes and the decay amplitudes into the $K^+\Lambda$ channel for several nucleon states, as predicted by Capstick and Roberts, are listed. Only those resonances are displayed that have significant photon– as well as $K^+\Lambda$ coupling based on the strength of the product

$$\chi_\lambda = \Gamma_{K\Lambda}^{1/2} A_\lambda / \Gamma_0 \tag{5}$$

[2]The expressions of all single and double polarization observables are listed in Appendix A.

where A_λ is the electromagnetic excitation amplitude $\gamma N \rightarrow N^*$ for helicity λ, Γ_0 and $\Gamma_{K\Lambda}$ are the total and the $K\Lambda$ decay widths, resp., for a given N^*. From these predictions it is expected that the two-star state $N\frac{3}{2}^-(1960)[D_{13}]_3$ will be identified clearly, and significant contributions from the other states will be observed in the reaction $\gamma p \rightarrow K^+\Lambda$.

Model state	$N\pi$ state	$A_{\frac{1}{2}}$	$A_{\frac{3}{2}}$	$A_{K\Lambda}$
$N\frac{1}{2}^-(1945)[S_{11}]_3$	$N(2090)^*$	12		2.3 ± 2.7
$N\frac{3}{2}^-(1960)[D_{13}]_3$	$N(2080)^{**}$ (?)	36	-43	$-5.6^{+1.7}_{-1.3}$
$N\frac{3}{2}^-(2055)[D_{13}]_4$	$N(2080)^{**}$ (?)	16	0	$-2.7^{+0.9}_{-0.8}$
$N\frac{5}{2}^-(2080)[D_{15}]_2$		-3	-14	$-2.9^{+0.8}_{-0.4}$
$N\frac{7}{2}^-(2090)[G_{17}]_1$	$N(2190)^{****}$	-34	28	$-1.3^{+0.4}_{-0.6}$
$N\frac{5}{2}^-(2095)[D_{15}]_3$		-2	-6	$-1.7^{+0.5}_{-0.4}$
$N\frac{9}{2}^+(2345)[H_{19}]_1$	$N(2220)^{****}$	-29	13	-0.4 ± 0.1
$N\frac{7}{2}^+(2390)[F_{17}]_2$		-14	-11	-1.7 ± 0.4

Table 1: Photoproduction amplitudes and decay amplitudes into the $K\Lambda$ channel for some negative-parity excited nucleon states according to the constituent quark model of Capstick and Roberts. Amplitudes are in units of 10^{-3} GeV$^{-\frac{1}{2}}$. Data taken from references [2] and [3].

In the phenomenological description of the reaction, two recent developments have represented important progress. A coupled-channels calculation that includes final-state interactions has linked the photoproduction process $p(\gamma, K^+)\Lambda$ to the hadronic process $p(\pi^-, K^0)\Lambda$ [17]. This unitary coupled-channels framework allows separating background from resonance contributions. Also, the inclusion of hadronic form factors at the hadronic vertices in photoproduction reactions while maintaining gauge invariance, has resulted in a proper description of the background terms using values for the leading coupling constants close to the values coming from SU(3) symmetry [18].

A recent calculation by Mart and Bennhold [5] based on the tree-level isobar model of Ref. [19], has found that in order to describe the structure around $W = 1.9$ GeV in the $p(\gamma, K^+)\Lambda$ data from SAPHIR, it is necessary to include the contribution of the $D_{13}(1960)$ resonance predicted by the quark model. Evidence for the existence of this resonance has also surfaced in two separate analyses of $p(\pi^-, K^0)\Lambda$ data [20, 21]. In Fig. 5, the results of the calculation with and without the contribution of the $D_{13}(1960)$ state are compared with the SAPHIR data. Fig. 6 shows the predictions for the target asymmetry T_y with and without contributions of the $D_{13}(1960)$ state, followed by the predictions for recoil polarization P_y and beam asymmetry Σ_x in Fig. 7. The results show that the influence of the new state in the recoil polarization is very small for all angles which demonstrates that this observable is not appropriate for further study of this resonance. On the other hand, beam and target asymmetry show much larger variations between the two calculations.

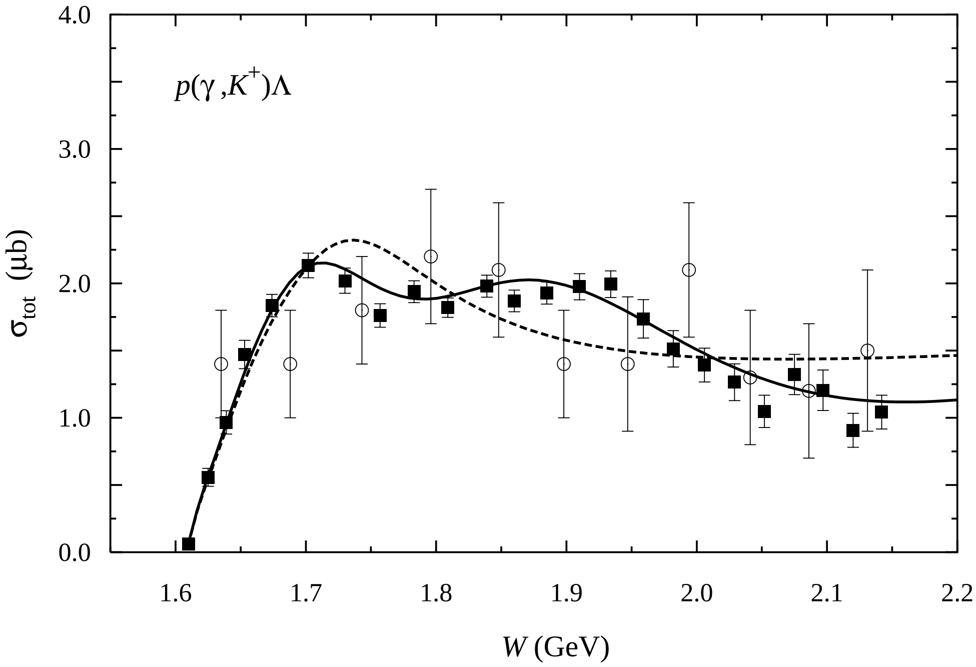

Figure 5: Total cross section for $K^+\Lambda$ photoproduction on the proton. The dashed line shows the model without the $D_{13}(1960)$ resonance, while the solid line is obtained by including the $D_{13}(1960)$ state. The new SAPHIR data [4] are denoted by the solid squares, previous data are shown by the open circles. Taken from Ref. [5].

The evidence for the existence of the $D_{13}(1960)$ resonance has been strengthened by the analysis of the new data on kaon electroproduction from Hall C at Jefferson Lab [22]. An extension of the isobar model of Bennhold and Mart to finite Q^2 shows that without the presence of the $D_{13}(1960)$ the data can not be explained[23].

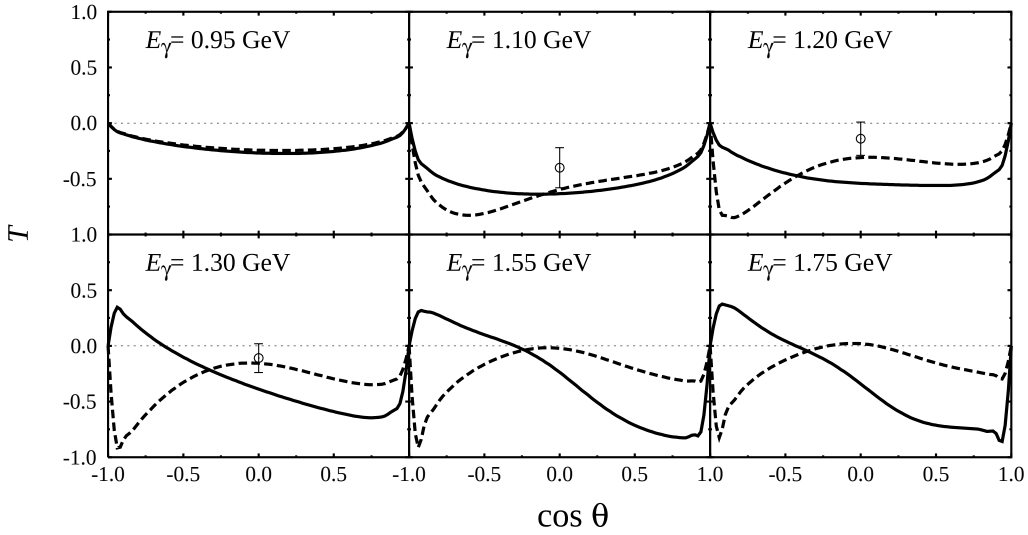

Figure 6: Target asymmetry T_y for $\gamma p \to K^+\Lambda$. The dashed line shows the model prediction [5] without the $D_{13}(1960)$ resonance, while the solid line is obtained by including the $D_{13}(1960)$ state. Experimental data from [7].

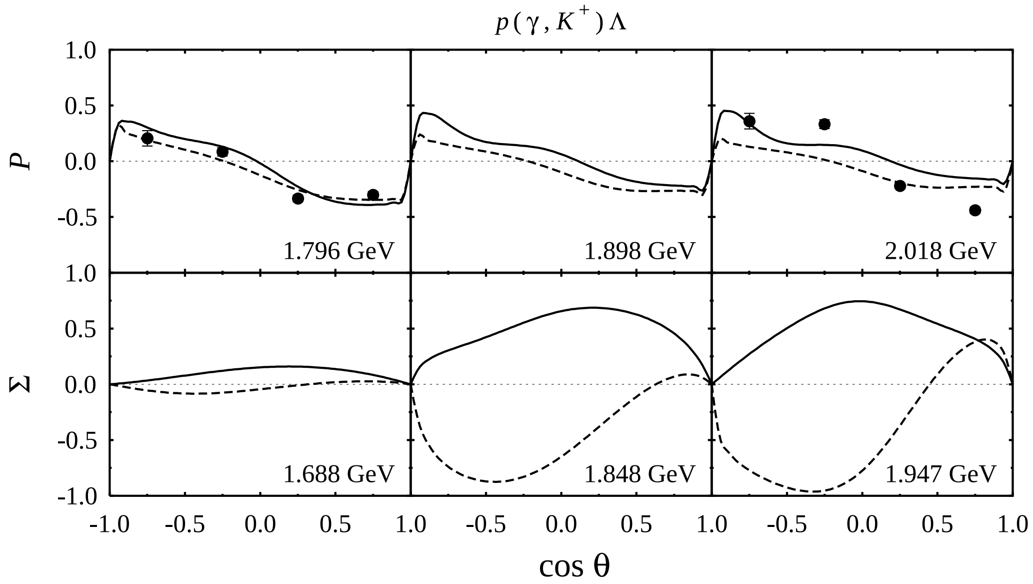

Figure 7: Recoil polarization R_y and beam asymmetry Σ_x for $\gamma p \to K^+\Lambda$. The dashed line shows the model prediction [5] without the $D_{13}(1960)$ resonance, while the solid line is obtained by including the $D_{13}(1960)$ state. Experimental data from SAPHIR [4].

One conclusion of these studies is that measurements of the beam and target asymmetry for $K^+\Lambda$ photoproduction will be an excellent way (and maybe the only way) to elucidate the contribution of various N^* resonances to this channel; resonances that may yet be undiscovered.

Experimental data using a polarized target and polarized photon beams up to E_γ=4.0 GeV will enable us to search not only for additional higher resonant states as predicted by the $^3P_0$ quark model (cf. Table 1), but also to investigate the transition between low– and high–energy hyperon production.
The partial wave analysis of $\gamma p \to K^+\Lambda$ up to photon energies above 2 GeV [13] may bridge the gap between the low- and high-energy regions as was recently shown for pion photoproduction [24] and NN elastic scattering [25].

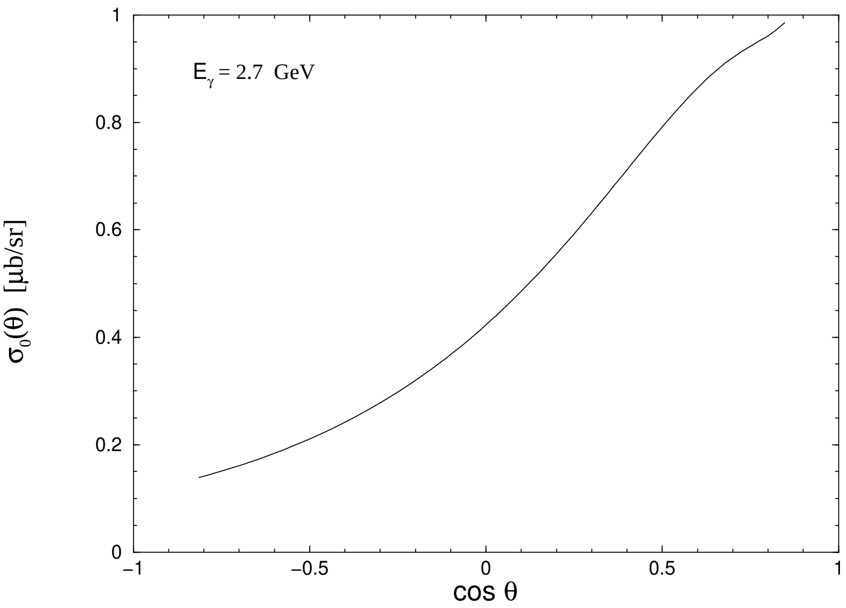

Figure 8: Regge model prediction for the differential cross section of $\gamma p \to K^+\Lambda$ at $E_\gamma = 2.7$ GeV. Calculation based on [26].

The general shape of the $K^+\Lambda$ photoproduction cross section above 2 GeV appears to be consistent with a high–energy behavior suggested by the Regge trajectory exchange model of J.M. Laget and M. Guidal [26] which describes the 4 GeV data of Anderson [8] predicting an energy dependence of s^{-3} at $\theta_{cm}(K^+) = 90°$. This model overestimates the cross section for $E_\gamma < 3.0$

GeV by more than 200 % (cf. figures 1 and 8).[3]

With the measurement of several polarization observables, including double polarization observables, an accurate description of the reaction will be achieved, and this will facilitate a partial wave analysis of the resulting data in order to identify the contributing resonances. The partial wave analyses of $K^+\Lambda$, $K^+\Sigma^0$ and $K^0\Sigma^+$ photoproduction require improved data for all energies in order to reduce the constraints for the PWA, and to extend the analysis to higher energies. Polarization observables are important for distinguishing resonance contributions from other (non-resonant) production dynamics.

5 Frozen Spin Polarized Target for CLAS

We propose to build a frozen spin target for use in photon-induced experiments with CLAS. The dynamically polarized target used for electron-beam experiments has the disadvantage that is requires the target to be located inside a strong (≈ 5 T) and very uniform (ΔB/B$\approx 10^{-4}$) magnetic field. The magnet needed to produce this field occupies a major fraction of the space around the target sample, leaving only a relatively small acceptance for outgoing particles, and the useful acceptance for low-momentum charged particles may be further reduced by large deflections in the magnetic field. For experiments using a large-aperture spectrometer like CLAS in conjunction with a tagged photon beam, which deposits negligible energy in the target, a more attractive option is to use a frozen spin polarized target.

In a frozen spin target, the material is polarized in the standard way with microwave irradiation in a high magnetic field. Then, with the microwaves off, the temperature of the material is lowered as much as possible, so that the relaxation time of the polarization becomes very long, hence the term "frozen spin". The value of the relaxation time is a strong function of the ratio B/T where B is the value of the magnetic holding field and T the material temperature. By operating at a sufficiently low temperature, it is possible to reduce the holding field to $< 0.5T$ and modest uniformity, while still preserving a high polarization for times acceptable for running the experiment.

The low holding field can be supplied either by the fringe field of the polarizing magnet or by another magnet, the geometry of which can be tailored to the particular experiment to provide a much larger acceptance than obtainable with a high-field magnet. For example, the polarized target for the Bonn–Mainz GDH experiments [28] uses a longitudinal holding field produced by a very

[3] We will include predictions for polarization observables where these can be extracted from the model.

thin (500μm) supperconducting solenoid located within the target cryostat which offers virtually no obstruction to the outgoing particles. Another arrangement may be solenoids in a certain distance from the target along the beam axis which do not obstruct the geometrical acceptance of the spectrometer. For transverse polarization, a suitable holding field could be produced by a pair of superconducting Helmholtz coils parallel to the beam axis, also contained within the target cryostat. Figure 9 shows a rough sketch of the holding magnets envisioned for CLAS. The coils could be positioned as much as possible within the shadows of the CLAS torus, to minimize he loss of acceptance.

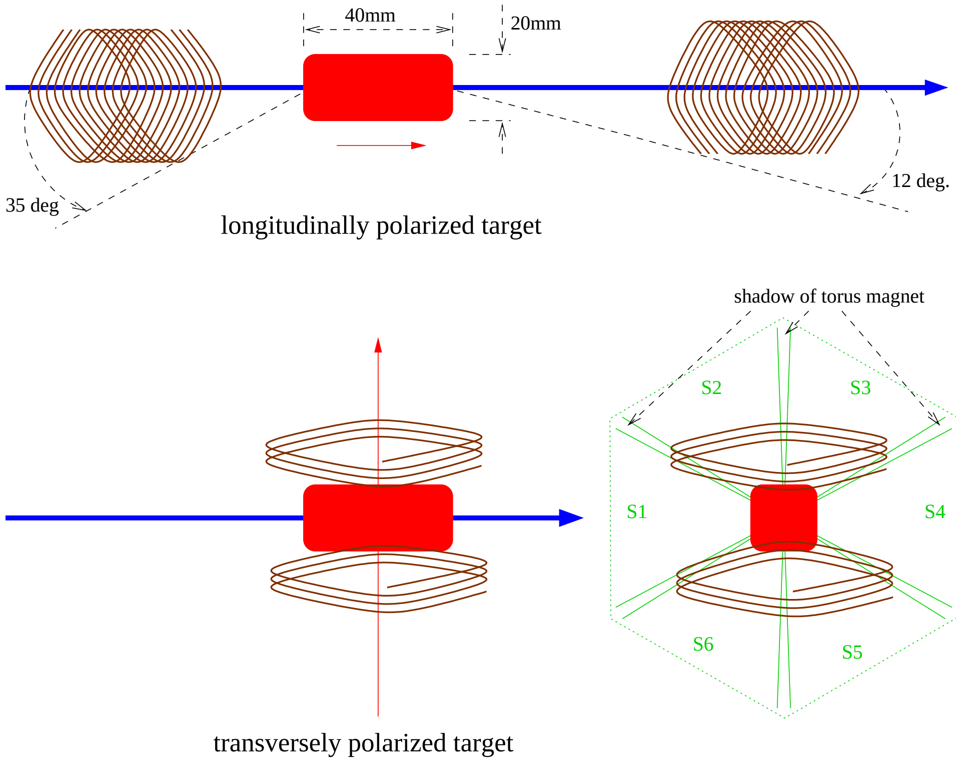

Figure 9: Sketch of the frozen spin target for CLAS.

A "standard" frozen spin target such as the Bonn–target uses butanol as target material. Another possible target material is polyethylene doped with TEMPO, which has similar dilution factor and polarization properties but allows a more accurate measurement of the effective thickness of the target beads. For the purpose of rate calculations, we propose to construct a cylindrical CH_2 target of 40 mm length and 20 mm diamter, with a density of 0.9 g/cm^3 and a free proton density of 0.8×10^{22} protons/cm^3.

A dilution refrigerator is used to provide the lowest temperatures and reasonable cooling power when polarizing. Typical values [29] would be 50 mK for frozen spin operation and 200–400 mK with ≈ 50 mW cooling power when polarizing. the University of Virginia (UVa) has the capability of providing such a refrigerator which can be assembled from major components currently in its laboratory. This dilution refrigerator was fabricated at CERN but never assembled; however, three others of the same design have been used very successfully in other experiments at the CERN PS and LEAR.

Other typical parameters for the system are [30]:
a 2.5 T polarizing magnet, microwave frequency of 70 GHz to polarize, and a standard Liverpool Q-meter would measure the polarization to a precision of about 3 %. For a butanol target, proton polarizations of about 90 % with hold times of around 200 hours are achievable, while deuteron polarizations for deuterated butanol could reach 50 % with long hold times.

This target system could efficiently be produced by a collaboration between the Jefferson Lab target group and UVa, and – especially if transverse polarizations are accommodated, would be a flexible facility for a wide range of polarization experiments with CLAS.

A Polarization observables in Kaon Photoproduction

As shown in fig. 4, the four-momenta of the incoming photon (γ), outgoing kaon (K), target proton (p), and recoiling hyperon (Y) are named p_γ, p_p, p_K, and p_Y, respectively. The variables in the center-of-mass system are written as $p_\gamma = (\nu, \vec{k})$, $p_K = (E_K, \vec{q})$, $p_p = (E_p, -\vec{k})$, and $p_Y = (E_Y, -\vec{q})$. The Mandelstam variables s, t, and u, are defined by

$$s = (p_p + p_\gamma)^2 = (p_K + p_Y)^2, \quad t = (p_\gamma - p_K)^2, \quad u = (p_p - p_K)^2 \ . \tag{6}$$

In the following definitions the differential cross section is abbreviated by

$$\sigma(B,T,R) \equiv \frac{d\sigma^{(B,T,R)}}{d\Omega}$$

where the superscripts denote:

B the polarization state of the photon <u>beam</u>: linearly ($\perp, \|, \pi/4$) or circularly ($\lambda_\gamma = \pm 1$);

T the polarization state of the proton <u>target</u>: spin orientation in the c.m. frame (x, y, z);

R the polarization state of the <u>recoiling</u> hyperon: spin orientation in the rest frame of the recoiling hyperon (x', y', z').

A.1 Single Polarization observables

Recoil polarization: $\mathbf{P} = \frac{\sigma(0,0,+y')-\sigma(0,0,-y')}{\sigma(0,0,+y')+\sigma(0,0,-y')}$

Beam polarization: $\mathbf{\Sigma} = \frac{\sigma(\perp,0,0)-\sigma(\|,0,0)}{\sigma(\perp,0,0)+\sigma(\|,0,0)}$

Target polarization: $\mathbf{T} = \frac{\sigma(0,+y,0)-\sigma(0,-y,0)}{\sigma(0,+y,0)+\sigma(0,-y,0)}$

A.2 Double Polarization Observables

A.2.1 Beam – Target Polarization

circ. beam – target$_x$ polar.: $\mathbf{E} = \frac{\sigma(+1,+z,0)-\sigma(-1,+z,0)}{\sigma(+1,+z,0)+\sigma(-1,+z,0)}$

circ. beam – target$_x$ polar.: $\mathbf{F} = \frac{\sigma(+1,+x,0)-\sigma(-1,+x,0)}{\sigma(+1,+x,0)+\sigma(-1,+x,0)}$

lin. beam – target$_z$ polar.: $\mathbf{G} = \frac{\sigma(\pi/4,+z,0)-\sigma(\pi/4,-z,0)}{\sigma(\pi/4,+z,0)+\sigma(\pi/4,-z,0)}$

lin. beam – target$_x$ polar.: $\mathbf{H} = \frac{\sigma(\pi/4,+x,0)-\sigma(\pi/4,-x,0)}{\sigma(\pi/4,+x,0)+\sigma(\pi/4,-x,0)}$

A.2.2 Beam – Recoil Polarization

circ. beam – recoil$_{x'}$ polar.: $\mathbf{C_{x'}} = \frac{\sigma(+1,0,+x')-\sigma(-1,0,+x')}{\sigma(+1,0,+x')+\sigma(-1,0,+x')}$

circ. beam – recoil$_{z'}$ polar.: $\mathbf{C_{z'}} = \frac{\sigma(+1,0,+z')-\sigma(-1,0,+z')}{\sigma(+1,0,+z')+\sigma(-1,0,+z')}$

lin. beam – recoil$_{x'}$ polar.: $\mathbf{O_{x'}} = \frac{\sigma(\pi/4,0,+x')-\sigma(\pi/4,0,-x')}{\sigma(\pi/4,0,+x')+\sigma(\pi/4,0,-x')}$

lin. beam – recoil$_{z'}$ polar.: $\mathbf{O_{z'}} = \frac{\sigma(\pi/4,0,+z')-\sigma(\pi/4,0,-z')}{\sigma(\pi/4,0,+z')+\sigma(\pi/4,0,-z')}$

A.2.3 Target – Recoil Polarization

transv. target – recoil$_{x'}$ polar.: $\mathbf{T_{x'}} = \frac{\sigma(0,+x,+x')-\sigma(0,+x,-x')}{\sigma(0,+x,+x')+\sigma(0,+x,-x')}$

transv. target – recoil$_{z'}$ polar.: $\mathbf{T_{z'}} = \frac{\sigma(0,+x,+z')-\sigma(0,+x,-z')}{\sigma(0,+x,+z')+\sigma(0,+x,-z')}$

long. target – recoil$_{x'}$ polar.: $\mathbf{L_{x'}} = \frac{\sigma(0,+z,+x')-\sigma(0,+z,-x')}{\sigma(0,+z,+x')+\sigma(0,+z,-x')}$

long. target – recoil$_{z'}$ polar.: $\mathbf{L_{z'}} = \frac{\sigma(0,+z,+z')-\sigma(0,+z,-z')}{\sigma(0,+z,+z')+\sigma(0,+z,-z')}$

B Polarization observables in terms of CGLN amplitudes

The polarization observables can be written in terms of the CGLN amplitudes [16]. The differential cross section is added because – in this theoretical framework – it is treated as a single polarization observable. The term ρ_o is defined as $\rho_o = |\vec{q}|/|\vec{k}|$.

$$\sigma_o(\theta) = \rho_o Re\{\ |f_1|^2 + |f_2|^2 - 2\cos\theta\ f_2 f_1^* + \frac{\sin^2\theta}{2}[\ |f_3|^2 + |f_4|^2 + 2 f_4 f_1^* + 2 f_3 f_2^* + 2\cos\theta\ f_4 f_3^*]\ \} \quad (7)$$

$$P_y(\theta) = \frac{\rho_o \sin\theta}{\sigma_o(\theta)}\ Im\{\ [2f_2 + f_3 + \cos\theta\ f_4]^*\ f_1 + f_2^*\ (\cos\theta\ f_3 + f_4) + \sin^2\theta\ f_3^* f_4\ \} \quad (8)$$

$$\Sigma_x(\theta) = -\frac{\rho_o \sin^2\theta}{2\sigma_o(\theta)}\ Re\{\ |f_3|^2 + |f_4|^2 + 2[\ f_1^* f_4 + f_2^* f_3 + \cos\theta\ f_3^* f_4\ ]\ \} \quad (9)$$

$$T_y(\theta) = \frac{\rho_o \sin\theta}{\sigma_o(\theta)}\ Im\{\ f_1^* f_3 - f_2^* f_4 + \cos\theta\ (f_1^* f_4 - f_2^* f_3) - \sin^2\theta\ f_3^* f_4\ \} \quad (10)$$

$$O_{x'}(\theta) = \frac{\rho_o \sin\theta}{\sigma_o(\theta)}\ Im\{\ f_2 f_3^* - f_1 f_4^* + \cos\theta\ (f_2 f_4^* - f_1 f_3^*)\ \} \quad (11)$$

$$O_{z'}(\theta) = -\frac{\rho_o \sin^2\theta}{\sigma_o(\theta)}\ Im\{\ f_1 f_3^* + f_2 f_4^*\ \} \quad (12)$$

References

[1] S. Capstick and N. Isgur, Phys. Rev. **D34**, 2809 (1986).

[2] S. Capstick and W. Roberts, Phys. Rev. **D49**, 4570 (1994).

[3] S. Capstick and W. Roberts, Phys. Rev. **D58**, 074011 (1998).

[4] SAPHIR Collaboration: M.Q. Tran *et al.*, Phys. Lett. **B445**, 20 (1998).

[5] T. Mart and C. Bennhold, Phys. Rev. **C61**, 012201 (2000).

[6] R.L. Anderson *et al.*, Phys. Rev. Letters **9**, 131 (1962); C.W. Peck, Phys. Rev. **135**, 830 (1964); A.J. Sadoff *et al.*, Bull. Am. Phys. Soc. **9**, 23 (1964); R.L. Anderson *et al.*, Proc. Int. Symp. on electron and photon interactions, Hamburg, 1965, p. 203; S. Mori, Ph.D. thesis, Cornell University, 1966; H. Thom, a compilation, Phys. Rev. **151** 1322 (1966); N.B. Mistry *et al.*, Phys. Lett. B **24** 528 (1967); D.E. Groom, J.H. Marshall, Phys. Rev. **159**, 1213 (1967); A. Bleckmann *et al.*, Z. Phys. **239**, 1 (1970); T. Fujii *et al.*, Preprint (INS, Univ. of Tokyo, 1970); P. Feller *et al.*, Nucl. Phys. B **39** 413 (1972); M. Grilli *et al.*, Nuovo Cim. **38** 1467 (1965); R. Haas *et al.*, Nucl. Phys. **B137** 261 (1978); D. Decamp *et al.*, L.A.L. 1236 (1970).

[7] G. Goeing, W. Schorch, J. Tietge, W. Weilenbock, Nucl. Phys. **B26**, 121 (1971).

[8] R.L. Anderson *et al.*, Phys. Rev. **D14**, 679 (1976).

[9] K. Abe *et al.*, Phys. Rev. **D32**, 2869 (1985).

[10] SAPHIR Collaboration: W.J. Schwille *et al.*, Nucl. Instrum. and Methods **A344**, 470 (1994).

[11] SAPHIR Collaboration: M. Bockhorst *et al.*, Z. Phys. **C63**, 37 (1994).

[12] TJNAF experiment E-89-004, spokesperson R. Schumacher.

[13] R. A. Arndt, I. I. Strakovsky, and R. L. Workman, work in progress, cf. http//:said.phys.vt.edu.

[14] G.F. Chew, M.L. Goldberger, F.E. Low, and Y. Nambu, Phys. Rev. **106**, 1345 (1957).

[15] G. Knöchlein, D. Drechsel, and L. Tiator, Z. Phys. **A352**, 327 (1995).

[16] C.G. Fasano, F. Tabakin, B. Saghai, Phys. Rev. **C46**, 2430 (1992).

[17] T. Feuster and U. Mosel, Phys. Rev. **C58**, 457 (1998); Phys. Rev. **C59**, 460 (1999).

[18] H. Haberzettl, Phys. Rev. **C56**, 2041 (1997); H. Haberzettl *et al.*, Phys. Rev. **C58**, R40 (1998).

[19] C. Bennhold, T. Mart, A. Waluyo, H. Haberzettl, G. Penner, T. Feuster, and U. Mosel, in *Proceedings of the Workshop on Electron Nucleus Scattering*, Elba, Italy, 1998, nucl-th/9901066 (1999); H. Haberzettl, C. Bennhold, T. Mart and T. Feuster, in *Proceedings of Baryons 98*, Bonn, Germany, 1998, nucl-th/9811024 (1998).

[20] D.H. Saxon *et al.*, Nucl. Ohys. **B162**, 522 (1980).

[21] K.W. Bell *et al.*, Nucl. Phys. **B222**, 389 (1983).

[22] G. Niculescu *et al.*, Phys. Rev. Lett. **81**, 1805 (1998).

[23] C. Bennhold, H. Haberzettl, T. Mart, invited talk at the *2nd ICTP International Conference on Perspectives in Hadronic Physics*, Trieste Italy, June 1998, nucl-th/9909022 (1999).

[24] D. A. Jenkins and I. I. Strakovsky, Phys. Rev. **C52**, 3499 (1995).

[25] R. A. Arndt, C. H. Oh, I. I. Strakovsky, R. L. Workman, and F. Dohrmann, Phys. Rev. **C56**, 3005 (1997).

[26] M. Guidal *et al.*, Nucl. Phys. **A627** 645 (1997); M. Guidal, J. M. Laget, and M. Vanderhaegen, Phys. Rev. **C61**, 025204 (2000).

[27] R.A. Williams, C-R. Ji, S.R. Cotanch, Phys. Rev. **C46**, 1617 (1992).

[28] W. Meyer, in *Proceedings of the GDH2000 Symposium* Mainz, Germany, 2000, (World Scientific, 2001) p. 157.

[29] D.G. Crabb and W. Meyer, Ann. Rev. Nucl. Part. Sci. **47**, 67 (1997).

[30] H. Dutz *et al.* , NIM **A356**, 111 (1995).